J. Fluid Mech. (1979), *vol.* 93, *part* 4, *pp.* 781–797
Printed in Great Britain

A simple fluid-flow model of ground effect on hovering

By JAMES LIGHTHILL

(Received 5 January 1979)

Hovering motions, by which an animal (or a helicopter) in stationary fluid generates a downflow to support its weight, entail energy costs that include the *induced power* (power supplied to that downflow). The simplest classical model for induced power is the actuator-disk model. This paper shows how a relatively insignificant modification can be made to that model to make it aerodynamically self-consistent. The modified simple model of the downflow may be evaluated in fluid that either is unbounded or is bounded below by horizontal ground. Comparison of the calculated induced powers in the two cases (even though made in this paper not for the true axisymmetric flow patterns but for the corresponding two-dimensional flow patterns) appears to give a more satisfactory analysis than was previously available of the observed reduction of induced power associated with proximity to the ground.

1. Introduction

It is well known that aerodynamic lift in forward motion carries an induced-drag penalty which is reduced near the ground. This 'ground effect' (significant in the performance of aircraft over a runway or of aquatic birds over a water surface) is well understood aerodynamically: wing downwash induced by trailing vortices is mitigated as a result of upwash induced by their 'images' in the ground.

It is equally well known that hovering in still air carries an induced-power penalty which is reduced near the ground (Zbrozek 1950; Bramwell 1976, pp. 101–3). This 'ground effect on hovering' was vital to early helicopters, many of which were inadequately powered for hovering to be possible except close to the ground. On the other hand, aerodynamic understanding of ground effect on hovering is far less developed than for forward flight; perhaps, because of its reduced significance for modern helicopters with their good power–weight ratios.

More recent studies of animal hovering (Weis-Fogh 1973; Lighthill 1977) give a special emphasis to induced power as setting the main upper limit on size for animals capable of sustained hovering. In comparison, power required to overcome the frictional resistance to wing motions is subject to different *scaling*, so that it is important for smaller insects, while induced power dominates for birds and bats and larger insects. In the meantime, the power that can be exerted in aerobic conditions (that is, in sustained effort where oxygen supply is the limiting factor) has an opper limit of the order of 200 W per kg of muscle in insects, birds and bats; accordingly, the observed upper limit (around 0·02 kg) on the mass of animals capable of sustained hovering in still air† (in all three groups) is ascribed to induced power increasing faster than in proportion to the weight supported.

† Not, of course, to be confused with the ability of (say) kestrels to stay motionless in a light wind.

0022–1120/79/4297–7350 $02.00

On the other hand, larger flying animals are frequently observed to use the motions of hovering to support their weight for just very brief periods. For example, the majority of terrestrial birds in both take-off and landing make a few strokes of a 'normal hovering' motion with nearly horizontal wing beats to give weight support as either forward acceleration commences or deceleration is completed (Lighthill 1975). Furthermore, many birds respond to various 'emergencies' in flight by a brief 'burst' of hovering motion. Of course, muscle power output in the anaerobic conditions of 'burst' activity can reach values around 3 times the maximum sustainable output, and this is recognized as the principal factor allowing relatively larger birds to hover for brief periods. At a more refined level, however, it is desirable to distinguish between (i) birds for which bursts of hovering activity are possible independently of ground effect and (ii) birds possessing such ability only in the presence of a significant reduction of induced power due to ground effect.

Fish behaviour, too, may be influenced by ground effect on hovering. Many bottom-living fishes are able to support their excess of weight over buoyancy by pectoral-fin motions analogous to the wing motions of animals hovering in air. Blake (1979) observed how common were extended periods of such hovering immediately above the bottom. He related this to the advantages of hovering for observing both prey and predators (and for allowing a ready response in either case by rapid accelerations), combined with a reduction of power requirements due to ground effect.

The present study was motivated principally by a desire to refine the above animal-locomotion discussion; but also, secondarily, by a feeling that the well-established but inadequately understood existence of a substantial ground effect reducing hovering induced power must be regarded as a challenge to analyse the phenomenon by means of a suitable aerodynamic model.

We must not expect such a model to be a simple extension of the classic model for ground effect in forward flight, since hovering is of a different aerodynamic nature. Indeed, the main previous attempt at a model (Knight & Hefner 1941) uses a rather too closely parallel approach: it concentrates on the vortices generated at the tips of the rotor blades, and assumes that they lie on a vertical cylinder bounding the rotor slipstream; essentially, just as they would in the absence of ground. It is then the images of those vortices in the ground which are taken to generate an upwash at the rotor disk and so reduce the induced power. Aerodynamically, the model is unsatisfactory because it allows for no growth in the diameter of the slipstream as it approaches the ground;† yet induced power is known to be highly sensitive to change in slipstream diameter; as, indeed, the model described in the next section will re-emphasize.

2. Model selection, assumptions and results

In order to obtain a satisfactory model of ground effect on the reduction of hovering induced power, it is essential to start from a model for induced power in the absence of ground that satisfies two conditions:

(i) it is aerodynamically self-consistent;

(ii) it is simple enough to be still usable with the ground added.

Under these conditions, the *ratio* C_P between the induced-power penalty for supporting

† Evidently, any vorticity near the ground must suffer a large outward movement, induced both by vortices near the rotor and by their images.

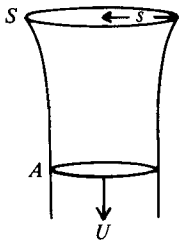

FIGURE 1. In this classical axisymmetric model, the slipstream from the actuator disk of area S becomes a vertical jet of reduced area A.

a given weight with and without ground effect may be adequately inferred even if the model's simplicity makes absolute induced powers somewhat in error.

The classical model for hovering induced power which most obviously offers the advantage of simplicity is the actuator-disk model. That model has the additional advantage for the purposes outlined in § 1 that it is applicable equally to helicopter hovering and animal hovering. The spinning rotor, or else the animal's oscillating wings or fins, is in each case represented as a disk of radius the semi-span s, from which a well-defined slipstream emerges. The slipstream has acquired a total head† in excess of that of the ambient fluid; which, in turn, in the region adjacent to the slipstream, remains essentially undisturbed (figure 1).

The theory, easy to work out for any radial distribution of total head in the slipstream, is known to give minimum induced power in the simplest case: when the total head in the slipstream is uniform (Glauert 1935). This simple model corresponds to the assumption that all fluid crossing the disk receives a uniform increase of pressure, equal to the disk loading:

$$\Delta p = W/S, \tag{1}$$

where W is the weight supported and $S = \pi s^2$ is the disk area.

In that case we may define a velocity U such that

$$\Delta p = \tfrac{1}{2}\rho U^2, \tag{2}$$

where ρ is the density of the fluid. This increase (2) in total head above that of the ambient fluid then implies that slipstream fluid immediately adjacent to (and therefore at the same pressure as) undisturbed ambient fluid is moving at speed U.

Admittedly, near the actuator disk, streamline curvature may allow transverse pressure gradients across streamlines, so that the uniform total head need not there imply a uniform fluid speed. Far below the actuator disk, however, such curvature must

† Throughout this paper the common expression 'total head' is used for the Bernoulli constant, obtained by adding the pressure to the fluid energy (kinetic plus potential) per unit volume.

disappear (figure 1), and the slipstream become a vertical jet of velocity U and cross-section

$$A = \tfrac{1}{2}S; \tag{3}$$

a value inferred from (1) and (2) and the requirement

$$\rho U^2 A = W \tag{4}$$

that the jet's momentum flux $\rho U^2 A$ must exactly support the weight W.

Next, the volume flow Q in the slipstream is given as

$$Q = UA. \tag{5}$$

Finally, the induced power P_i (rate of working on the slipstream by the actuator disk) is

$$P_i = (\Delta p)\, Q, \tag{6}$$

a result which equations (1) to (5) allow us to rewrite in the well-known form

$$P_i/W = \tfrac{1}{2}U = (W/2\rho S)^{\frac{1}{2}}, \tag{7}$$

usually taken to represent a lower limit for induced power per unit supported weight. Note that this increases as the square root of the disk loading W/S; which in turn, for geometrically similar systems, increases progressively with size, producing in hovering animals the intensification of induced-power problems as a function of size referred to in § 1.

The actuator-disk model, being axisymmetric, can be regarded as a model of the flow with all azimuthal variations smoothed out. This means that the slipstream flow, as a steady axisymmetric motion with uniform total head, is necessarily *irrotational*; a conclusion readily proved from 'Crocco's relation' (see, for example, Batchelor 1967, p. 160), which equally shows that the slipstream boundary (a discontinuity of total head) is a *vortex sheet*. Physically, this is because the assumption of uniform disk loading requires the rotor blades (or wings, or fins) to shed trailing vorticity only at their tips. A smoothed effect of that complex pattern of tip vortices is the actuator-disk-theory vortex sheet, of uniform strength U.

On the other hand, the contraction of that vortex sheet from the disk area S to a reduced cross-section A represents a real phenomenon, observable by flow visualization (Bramwell 1976, p. 118). Similarly, more accurate theories of the vorticity pattern predict that such a contraction occurs; see Theodorsen (1969) for the helical vortex pattern shed by a rotor, or Rayner (1979) for the stack of vortex rings shed by a hovering animal. Typical departures from the value (7) for induced power, either as measured, or as calculated in these more complicated theories, are of the order of 10–20 per cent.

The above considerations suggest as a potentially useful goal the extension of actuator-disk theory to allow for the presence of horizontal ground at a height h below the disk. The object would be to calculate, for support of a fixed weight W, the ratio

$$C_P = \frac{\text{induced power with ground effect}}{\text{induced power without ground effect}} \tag{8}$$

as a function of the ratio h/s of height to semi-span. Before that programme can be carried out, however, one small refinement of classical actuator-disk theory is needed, to make it aerodynamically self-consistent.

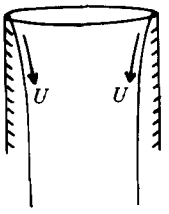

FIGURE 2. An aerodynamically self-consistent form of the axisymmetric actuator-disk model.

The reason for this is as follows. No new fluid is created at the actuator disk; which, indeed, is a source *not* of mass flux but of momentum flux. Thus, the whole volume flow Q emerging in the slipstream has been drawn from the general ambient fluid towards the disk's upper side, and there given the total-head increase Δp. This flow inward towards the disk's upper side must be an *irrotational* motion (again, with uniform total head), which at large distances from the disk has the character of an inwardly directed 'sink' flow.† Evidently, some of this inflow into the disk's upper surface must come from the region below the disk. This, however, is inconsistent with the fact that motion of ambient fluid immediately outside the slipstream has been excluded in the theory's assumptions.

Quantitatively, this inconsistency may not be too significant, since the sink flow velocities fall off as the inverse square of the distance. We cannot, however, ignore the inconsistency: for one thing, its significance may be greatest in the important region of slipstream contraction; and, furthermore, an aerodynamically consistent theory should offer better chances for a proper incorporation of ground effect.

Fortunately, the inconsistency in the model is eliminated rather easily by inserting an artificial boundary to shield the slipstream from the sink flow outside it. Out of all possible shapes of artificial boundary, one stands out as uniquely appropriate: a boundary in the form of a vertical cylinder (figure 2). The fluid motion, then, is the uniquely defined irrotational flow which emerges from the region outside that semi-infinite cylinder and, inside it, is bounded by a free stream surface on which the fluid speed has the constant value U.

It might be imagined that such use of a vertical boundary in the model is responsible for the fact that some fluid approaches the actuator disk from below. In reality, however, the whole concept of the actuator disk in still air requires some of the fluid entering the disk to approach it from below, and the introduction of the vertical boundary merely limits the region from which such fluid appears.

The idea that the artificially introduced boundary must be *vertical* is first indicated by the required contraction ratio $\frac{1}{2}$ (ratio of jet cross-section to disk area). This at once recalls 'Borda-mouthpiece' flow (known to have contraction ratio $\frac{1}{2}$) which is exactly the flow illustrated in figure 2. Admittedly, the classical 'Borda-mouthpiece' flow (Lamb 1932, p. 25) is a motion of fluid *all* of which is at a total head greater by $\frac{1}{2}\rho U^2$ than the undisturbed fluid adjacent to the jet. The flow of figure 2 is different in that

† This inescapable conclusion for an actuator disk in stationary fluid differs, of course, from the corresponding conclusion in the other classical actuator-disk theory; that for a propeller in a uniform stream. The motion towards the disk is there a combined sink-and-uniform-stream motion.

the increase in total head by $\frac{1}{2}\rho U^2$ takes place only at the disk itself. However, both are irrotational motions satisfying identical boundary conditions; therefore, their streamlines must be the same.

Two arguments suggest why the artificially introduced boundary should indeed be taken vertical. First, it allows a satisfactorily extensive region of fluid (all the fluid outside the semi-infinite cylinder) to participate in the sink flow. The second, much more compelling argument is that a vertical boundary cannot impart any vertical force to the fluid (or, indeed, in axisymmetric motion, any net force at all). There is therefore no disturbance to the basic assumption of actuator-disk theory, that the only force applied to the fluid is that associated with a uniform pressure difference $\frac{1}{2}\rho U^2$ applied right across the disk.

It is worth repeating that the shape of the artificial boundary is significant only close to the disk (where suctions associated with acceleration towards the disk would allow a non-vertical boundary to exert a significant force). The actuator-disk model becomes aerodynamically satisfactory provided that a short piece of vertical-cylinder boundary is inserted near the disk. For full details of how the artificial boundary can best be represented in the model, see § 3.

The discussion up to this point suggests that an aerodynamically consistent model of ground effect on hovering will be obtained by calculating how the axisymmetric Borda-mouthpiece flow is modified by the presence of a ground plane at a height h below the orifice.† It might be possible, although no doubt extremely laborious, to make such a calculation; however, one further simplification of the model makes the calculation completely elementary.

The requisite simplification is to solve just the corresponding two-dimensional problem. The two-dimensional Borda-mouthpiece flow is well known (Lamb 1932, p. 96); the corresponding shape of free streamline (on which the fluid speed takes the constant value U) is that marked '∞' in figure 3. The corresponding free-streamline shapes (calculated in § 3) are also given for four finite values of the ratio h/s of height above ground to semi-span (the lowest of these, 0·6, represents something like a typical lower limit for practical values of h/s). Furthermore, figure 4 plots the ratio C_P defined in equation (8), as a function of h/s for this two-dimensional model.

The philosophy behind this extra simplification is that noted earlier: such a ratio C_P between induced powers with and without ground effect may be indicated fairly reliably if one and the same simple model is evaluated in both cases. Actually, however, even the absolute value of power–weight ratio without ground effect is unaffected by the simplification; it is still $\frac{1}{2}U$ in the two-dimensional case. That is because all the results (1) to (7) still hold in the two-dimensional case provided that the letters W, S, A and Q stand for values of weight supported, orifice area, jet area, and volume flow 'per unit breadth perpendicular to the paper'. It should, on the other hand, be noted that, where equation (3) making the contraction ratio $\frac{1}{2}$ implied a diameter contracting by $\sqrt{(\frac{1}{2})} = 0{\cdot}707$ in axisymmetrical flow, the same area contraction in two-dimensional flow (curve marked '∞' in figure 3) involves of course a halving of the diameter. (On the other hand, no simple relationship exists between other aspects of a two-dimensional flow and the corresponding axisymmetric flow.)

† From this point onwards (with the concentration upon 'mouthpiece' flows established) the word 'orifice' is used in preference to 'disk' for the location where the increase in total head by $\frac{1}{2}\rho U^2$ takes place.

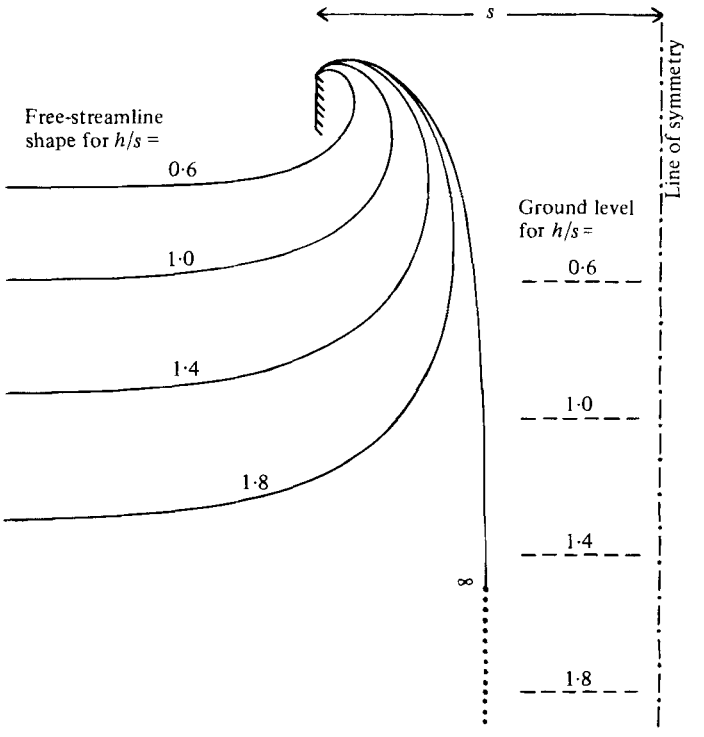

FIGURE 3. Calculated free streamlines in the two-dimensional model corresponding to that of figure 2, both without ground effect (curve marked '∞') and with ground effect for four different values of the ratio h/s of height above ground to half-orifice width.

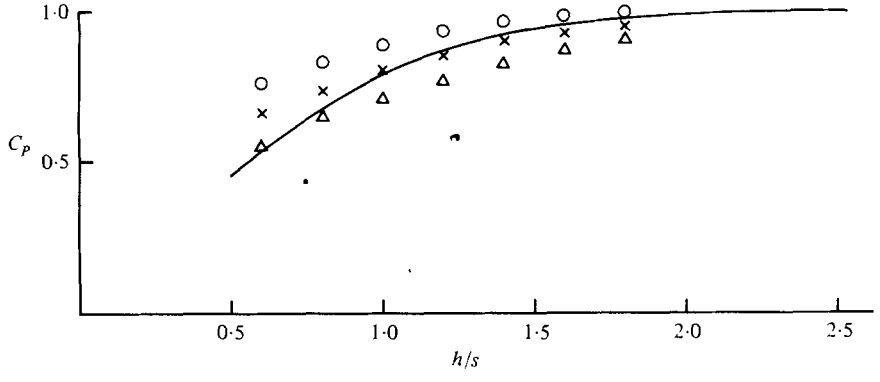

FIGURE 4. The induced power coefficient defined in equation (8), as a function of the ratio h/s of height above ground to half-orifice width. Experimental points: helicopter data (Zbrozek 1950) for different values of the ratio 'thrust coefficient to solidity': △, 0·025; ×, 0·05; ○, 0·1.

The experimental points on figure 4, taken from Zbrozek (1950) for helicopters, indicate that the model, besides being aerodynamically self-consistent, epresents the data about as well as any other single curve of C_P against h/s could do. A more refined model (for example, an extension of the Rayner (1979) vortex-ring model for hovering animals) would, of course, necessarily take other variables into account.

Interpreting physically the results in figures 3 and 4, we come across an apparent

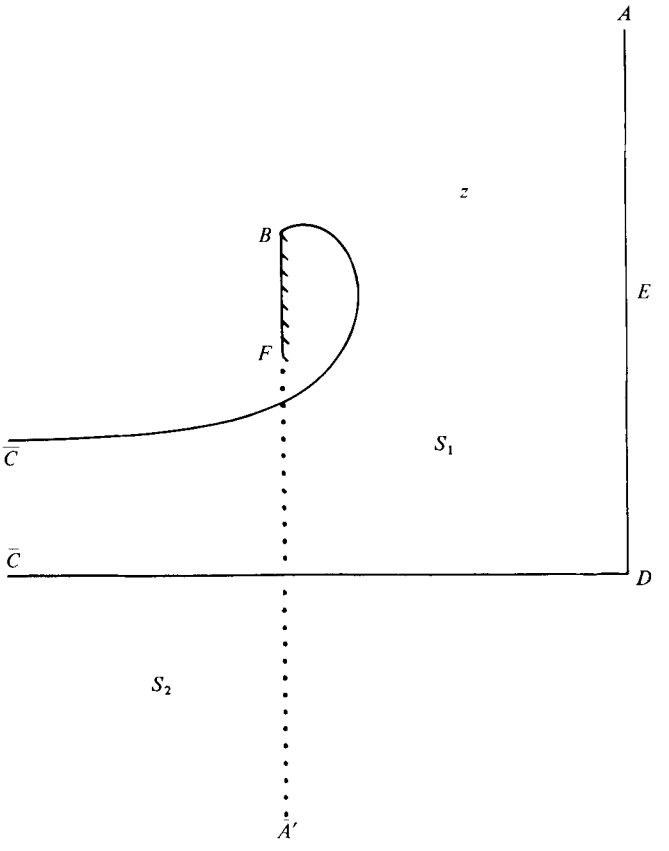

FIGURE 5. This figure illustrates just half of the two-dimensional model, for which the vertical AD is a line of symmetry. The line CD represents the ground and the curve BC the free streamline. To make the theory aerodynamically self-consistent, an artificial boundary BF is introduced as in figure 2. Its continuation FA' is on a different sheet S_2 of the Riemann surface from the main sheet S_1 on which the interaction of the slipstream with the ground takes place.

paradox, as follows. The classical theory of equations (1) to (7) associates the factor $\frac{1}{2}$ in the area contraction (3) with a corresponding factor $\frac{1}{2}$ in expression (7) for P_i/W (induced power per unit weight supported).† Including the ground reduces P_i/W by the additional factor $C_P < 1$; yet, paradoxically, the minimum cross-section of the jet is not so much reduced as in the case without ground.

The apparent paradox is resolved as follows. Without ground, the jet has minimum area A where it has already become straight and uniform; this leads to equation (4) relating that area to the weight supported. By contrast, ground effect causes the jet to reach its most contracted configuration where it is by no means uniform. There, streamline curvature requires pressures in the centre of the jet to be in excess of ambient values; accordingly, the fluid speed q is less than its free-streamline value U. In this case, the combined pressure force and momentum flux require a *greater* cross-section to achieve weight support than before; on the other hand, the substantially

† For P_i/W, by (1) and (6), is Q/S, which, if (5) were true with A as the jet's minimum area, would be $U(A/S)$; where, furthermore, U is fixed as $(2W/\rho S)^{\frac{1}{2}}$ by (1) and (2).

lowered fluid speeds q reduce the volume flux Q *more* than the greater cross-section increases it; and the induced power (6) falls by the same amount. For a precise mathematical form of this argument, see the end of § 3.

3. Details of the model

This final section, indeed, is devoted entirely to putting mathematical details on record. The two-dimensional flow field of our model (figure 5) is symmetrical about the line AD. Accordingly, it is sufficient to calculate the flow on (say) the left-hand side of AD, illustrated in figure 5. Here, AD itself is a dividing streamline, in which the velocity rises from very low values far from the orifice (at A) to a maximum at E and then falls to zero at the stagnation point D. The curve BC is a free streamline on which the pressures are simply hydrostatic. Since the flow is taken to be steady and irrotational, this implies that the fluid speed q takes a constant value U on the free streamline BC. The line CD represents the horizontal ground over which hovering takes place.

The fluid which is sucked into the orifice comes from a region bounded by the central streamline AE and by our artificially introduced boundary BF. As explained in § 2, some such artificially introduced boundary is needed in order that the flow of fluid drawn towards the orifice will not interfere with the hydrostatic conditions adjacent to the free streamline BC. The most important consideration dictating the choice of artificial boundary is that a vertical solid boundary introduced at BF cannot impart any net vertical force to the fluid (or, indeed, any force at all since the horizontal force between it and the fluid is cancelled by the equal and opposite horizontal force at its mirror image in the line of symmetry AD). Therefore, there is no disturbance to the model's basic assumption; the only force applied to the fluid is that associated with a uniform pressure difference $\frac{1}{2}\rho U^2$ (equation (2)) applied right across the orifice. Furthermore, the irrotationality of the motion is unaffected by this uniform increase in total head, except of course that the free streamline BC, as a surface of discontinuity between flow with that increased total head and stagnant fluid without it, is a vortex sheet.

The main effect of the artificial boundary BF on the properties of the jet must arise from its shape near B where the flow accelerates towards velocity U and the pressure drops below ambient pressure. That is where it is important for the artificial boundary to be vertical, so that it does not act on the jet with any net suction force. Beyond F, it is hardly important which shape we choose.

For the mathematical model, however, a particular mathematical concept suggests a continuation of the artificial boundary beyond F which is highly convenient for calculation purposes and, also, admirably avoids interference between the low-head flow moving towards the orifice and the high-head jet bounded by the free streamline BC. Briefly, we are able in the mathematical model to put those two flows on different sheets (S_2 and S_1) of a Riemann surface! The dotted line FA' in figure 5 shows the continuation of the artificial boundary BF on to a second sheet S_2 of the Riemann surface. Then flow enters the half-orifice at BE having been drawn from a wide expanse of low-head fluid in S_2, filling all space to the left of BA' and AE. Its head is increased by $\frac{1}{2}\rho U^2$ at BE, and thereafter it flows on the sheet S_1 which is where the presence of the ground CD can interfere with the jet motion.

It is important to notice that there is nothing unphysical about a solution of the two-

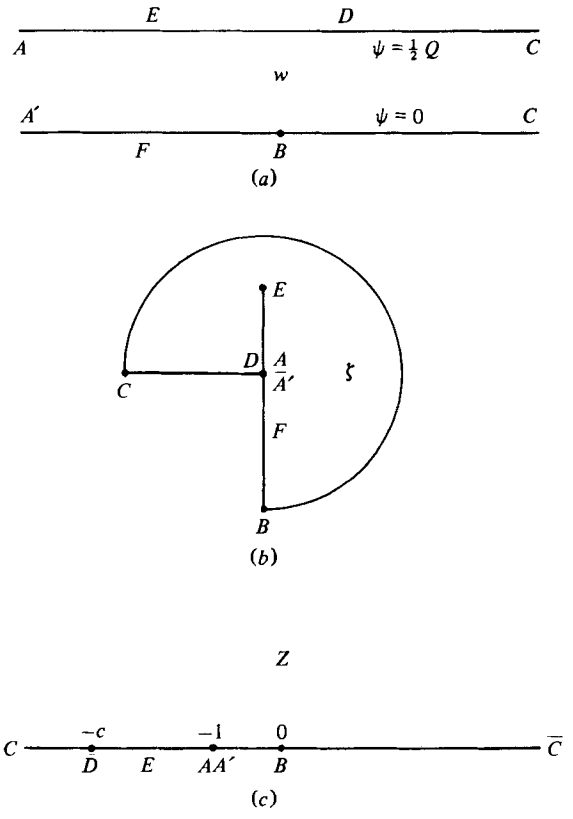

FIGURE 6. Auxiliary domains onto which the z-domain of figure 5 is mapped: (*a*) the w-domain, for which the mapping is the complex potential $w(z)$; (*b*) the ζ-domain, for which the mapping is the complex velocity $\zeta(z)$; (*c*) the Z-domain, which is simply the upper half Z-plane.

dimensional Laplace equation on such a Riemann surface. A quite simple physical model of such solutions makes this clear.

In this, we recognize the two-dimensional Laplace equation as correctly describing the flow between two parallel planes, at each of which slip is allowed, a distance δ apart. We interpret our solution in this sense on sheet S_1. However, in the transition to sheet S_2 (around the point F on figure 5, together with all points to the left of it) the model allows the central surface of the flow region to be warped gradually from its original plane configuration, and to continue to diverge from it until it reaches a new (and parallel) plane configuration S_2 a distance δ (or more) away. This distance is sufficient so that the flow in sheet S_2 will not meet the flow in S_1. Where the warping of the central surface is occurring, however, the sheet of fluid remains of constant thickness δ. Then, if the warping is gradual enough, the flow in such a channel (of uniform cross-section) continues to satisfy Laplace's equation. Furthermore, this physical model of our flow field does, in the limit as $\delta \to 0$, become geometrically a Riemann surface.†

† Yet another physical model would be exactly as above but with no slip at the walls. The theory of the Hele–Shaw apparatus shows that this, too, is a flow field satisfying Laplace's equation within a region whose geometry is that of our required Riemann surface.

With this model for our Riemann surface it seems physically reasonable to allow the fluid sucked into the orifice to come from all parts of S_2 to the left of BA'. Note, in particular, that the change expected from a more 'natural' model, which allows no flow from any such parts below the level of F, is likely to be small as far as the flow in S_1 is concerned. In the meantime, the actual model chosen has the strong advantage of avoiding any disturbance to the balance of vertical forces. Also, the configuration of the free streamline in S_1 should be only minimally influenced by the presence, on the different sheet S_2, of the artificially introduced boundary.

From the mathematical model we wish to relate the half-flux $\frac{1}{2}Q$ (volume flow of fluid through the half-orifice, per unit breadth 'perpendicular to the paper') to the half-orifice's width s and its height h above ground. To this end we use a complex potential w whose imaginary part ψ (the stream function) has boundary values $\psi = 0$ on the streamline $A'FBC$ and $\psi = \frac{1}{2}Q$ on the streamline $AEDC$. The analytic function $w(z)$ maps the z-domain of figure 5 into the w-domain of figure 6(*a*), bounded by the parallel lines $\psi = 0$ and $\psi = \frac{1}{2}Q$. The real part of w (the velocity potential ϕ) is made definite by requiring that $\phi = 0$ at the orifice lip B.

As in free-streamline problems generally, it is important to study also the analytic function $dw/dz = \zeta(z)$: the complex velocity. This has modulus $|\zeta|$ equal to the fluid speed q, and argument $\arg\zeta$ equal to $-\theta$, where θ is the direction of fluid flow. Therefore, $\zeta(z)$ maps the z-domain onto the ζ-domain of figure 6(*b*). Here, the free streamline BC, on which $q = U$, becomes an arc of the circle $|\zeta| = U$. The 'artificial' boundary $A'FB$, on which the flow direction θ is $+\frac{1}{2}\pi$, becomes the radius $\arg\zeta = -\frac{1}{2}\pi$. On the line of symmetry AED, the flow direction θ is $-\frac{1}{2}\pi$, but the greatest speed attained is necessarily less than U, so that AED becomes just part of the radius $\arg\zeta = +\frac{1}{2}\pi$. Finally, the streamline DC along the ground from the stagnation point D becomes the radius $\arg\zeta = \pi$.

We introduce one more auxiliary complex variable Z, defined by the exponential mapping

$$Z = e^{2\pi w/Q} - 1. \tag{9}$$

This mapping is used because it yields an extremely simple Z-domain: just the upper half of the Z-plane, as in figure 6(*c*). This point B where $w = 0$ maps into the origin $Z = 0$, while the points A and A' where $w = -\infty$ correspond to $Z = -1$. The point C where $w = +\infty$ becomes the 'point at infinity' in the Z-domain. The position of the point D in the Z-domain is *a priori* unknown, but must be to the left of A. We take $Z = -c$ at the point D, and will find that $c > 1$ is the principal parameter in our solution, in terms of which all other non-dimensional qualities are derived.

Classical methods† allow us to determine uniquely the mapping of the upper half Z-plane onto the ζ-domain of figure 6(*b*), with the points C, D, A and B in the two figures corresponding (but with the positions of E in both unrestricted). We obtain

$$\frac{dw}{dz} = \zeta = \left\{-U\frac{Z^{\frac{1}{2}}-i}{Z^{\frac{1}{2}}+i}\right\}\left[\frac{Z^{\frac{1}{2}}-ic^{\frac{1}{2}}}{Z^{\frac{1}{2}}+ic^{\frac{1}{2}}}\right]^{\frac{1}{2}}. \tag{10}$$

Here, $Z^{\frac{1}{2}}$ is the branch of the square root within the Z-domain that is positive for $Z > 0$, giving $|\zeta| = U$ on the free streamline CD. This branch of $Z^{\frac{1}{2}}$ is pure imaginary for $Z < 0$, with positive imaginary part. Accordingly, the square bracket in (10) is positive for $Z < -c$; and we take its square root, similarly, as the branch positive for $Z < -c$.

† For example, the Schwarz–Christoffel method applied to the variable $\log\zeta$.

As required, then, ζ is negative for $Z < -c$, and varies from 0 to $-U$ as Z goes from $-c$ to $-\infty$. Where $-c < Z < 0$, on the other hand, the square bracket in (10) becomes negative, while the branch of its square root that is positive for $Z < -c$ becomes pure imaginary, with *negative* imaginary part. That is why equation (10) makes $\arg\zeta$ equal to $+\frac{1}{2}\pi$ for $-c < Z < -1$, and to $-\frac{1}{2}\pi$ for $-1 < Z < 0$ (where the term in curly brackets is positive).

The relationship of the half-orifice width s and the height above ground h to the fluid-dynamic parameters U and Q is determined by calculating the complex variable $z = x + iy$ representing the position co-ordinates (x, y) of a point on the boundary of the z-domain. From equations (9) and (10) we have

$$z = \int \frac{dw}{\zeta} = \frac{Q}{2\pi}\int \frac{dZ}{\zeta(Z+1)}. \tag{11}$$

The integration in (11) can be carried out in terms of elementary functions, as

$$z = \frac{Q}{\pi U}\left\{ i\frac{c^{\frac{3}{2}}+2c-1}{(c-1)^{\frac{3}{2}}}\log\left[\frac{(Z+c)^{\frac{1}{2}}+(c-1)^{\frac{1}{2}}+Z^{\frac{1}{2}}-i}{(Z+c)^{\frac{1}{2}}-(c-1)^{\frac{1}{2}}+Z^{\frac{1}{2}}-i}\right] \right.$$
$$\left. -\log\left[(Z+c)^{\frac{1}{2}}+Z^{\frac{1}{2}}\right]-\frac{(Z+c)^{\frac{1}{2}}}{(c^{\frac{1}{2}}-1)\,(Z^{\frac{1}{2}}-i)}\right\}+\text{constant}. \tag{12}$$

The reader may check this statement by differentiating (12) with respect to Z and retrieving $Q/[2\pi\zeta(Z+1)]$ with ζ given by (10). In (12), the square root $(Z+c)^{\frac{1}{2}}$ is taken positive for $Z > -c$; so that it becomes pure imaginary, with *positive* imaginary part, where $Z < -c$ (on the ground CD).

We can relate the half-orifice width s to the other parameters by considering the singular behaviour of (12) at $Z = -1$, corresponding to the change from A' to A. Two terms in (12) are singular at $Z = -1$. The last term in curly brackets becomes infinite as $Z \to -1$ either from above or below, but it is pure imaginary, tending respectively to $-i\infty$ or $+i\infty$ in these two cases. That corresponds to the positions of A' and A in the z-domain of figure 5. At the same time the denominator of the logarithm on the first line of (12) becomes zero. Admittedly, it is unimportant that the real part of the logarithm therefore tends to infinity, because it is multiplied by a pure imaginary factor; once again, then, only the imaginary part of z is thereby given a component tending to infinity (indeed, very slowly so that the previous singular term dominates). The important consideration is that the logarithm changes by $(-\pi i)$ between A' and A, as the singularity $Z = -1$, where the denominator inside the logarithm vanishes, is half-encircled in the positive sense. This specifies the half-orifice width s (change in the real part of z) as

$$s = \frac{Q}{U}\frac{c^{\frac{3}{2}}+2c-1}{(c-1)^{\frac{3}{2}}}. \tag{13}$$

An interesting check on equation (13) is obtained if we calculate the force F acting (per unit breadth perpendicular to the paper) upon the half-ground CD to the left of the line of symmetry. We obtain this as the integral from C to D of the steady-flow expression

$$P = \tfrac{1}{2}\rho(U^2 - q^2) \tag{14}$$

for the excess pressure (excess over hydrostatic). This gives

$$F = \tfrac{1}{2}\rho\int_C^D (U^2-\zeta^2)\,dz = \frac{\rho Q}{4\pi}\int_{-\infty}^{-c}\left(\frac{U^2}{\zeta}-\zeta\right)\frac{dZ}{Z+1}, \tag{15}$$

where (11) has been used to write the expression as an integral with respect to Z. The integral (15) is readily calculated from (10) as

$$F = \tfrac{1}{2}\rho Q U \frac{c^{\frac{3}{2}} + 2c - 1}{(c-1)^{\frac{3}{2}}}. \tag{16}$$

By (13), this makes the force F acting between the half-ground and the fluid equal to

$$F = \tfrac{1}{2}\rho U^2 s = \tfrac{1}{2}W; \tag{17}$$

namely, the downward force $\frac{1}{2}W$ (again, per unit breadth) exerted over the half-orifice width s by the pressure jump $\frac{1}{2}\rho U^2$. This agrees with the need for those two forces to balance, resulting from the fact that the rate of change of vertical fluid momentum is zero.

The induced power exerted over the full orifice width $2s$, per unit breadth perpendicular to the paper, is equal to the pressure jump $\frac{1}{2}\rho U^2$ times the volume flux Q, as in equation (6). The induced-power coefficient C_P is defined by (8) as the ratio of this induced power to its value $\frac{1}{2}UW$ given in the absence of ground effect by equation (7). Therefore, by (17) and (13),

$$C_P = \frac{\frac{1}{2}\rho U^2 Q}{\frac{1}{2}UW} = \frac{Q}{Us} = \frac{(c-1)^{\frac{3}{2}}}{c^{\frac{3}{2}} + 2c - 1}. \tag{18}$$

Equation (18) confirms that ground effect *reduces* induced power, by a factor $C_P < 1$ which depends only on the parameter c.

Now we determine the height h of the orifice above ground, in order to relate this parameter c to the ratio h/s. We calculate h from (12) as

$$h = \Big[\operatorname{Im} z\Big]_{+\infty}^{0} + \left(\frac{\frac{1}{2}Q}{U}\right). \tag{19}$$

Here, the first term is the change in y (the imaginary part of z) along the free streamline CB. The height of the jet at C, carrying flux $\frac{1}{2}Q$ at speed U, is given by the second term. (This value, obvious physically, could also be calculated from (12), where the logarithm on the second line changes at the 'point at infinity' C by $(-\frac{1}{2}\pi i)$ from $Z = -\infty$ to $Z = +\infty$.)

To calculate the first term in (19) we note that as $Z \to +\infty$ the whole expression in curly brackets in (12) becomes purely real. In fact, the first term tends to zero as $Z \to +\infty$; the second term is real for all $Z > 0$ (and tends to $-\infty$ as $Z \to +\infty$, corresponding to the free streamline's indefinite extension to the left); while the third term tends to a real constant as $Z \to +\infty$. Therefore, the change in $\operatorname{Im} z$ between $+\infty$ and 0 can be obtained by writing down the expression in curly brackets in (12) at $Z = 0$, giving

$$h = \frac{Q}{\pi U} \operatorname{Im}\left\{ i \frac{c^{\frac{3}{2}} + 2c - 1}{(c-1)^{\frac{3}{2}}} \log\left[\frac{c^{\frac{1}{2}} + (c-1)^{\frac{1}{2}} - i}{c^{\frac{1}{2}} - (c-1)^{\frac{1}{2}} - i}\right] - \log(c^{\frac{1}{2}}) - i\frac{c^{\frac{1}{2}}}{c^{\frac{1}{2}} - 1}\right\} + \frac{\frac{1}{2}Q}{U}. \tag{20}$$

This formula is readily simplified to

$$h = \frac{Q}{\pi U}\left\{\frac{c^{\frac{3}{2}} + 2c - 1}{(c-1)^{\frac{3}{2}}} \log\left[c^{\frac{1}{2}} + (c-1)^{\frac{1}{2}}\right] - \frac{c^{\frac{1}{2}}}{c^{\frac{1}{2}} - 1} + \tfrac{1}{2}\pi\right\}. \tag{21}$$

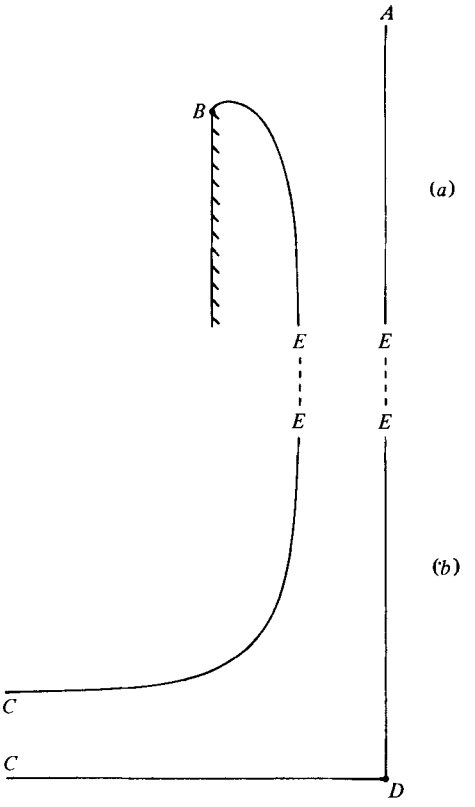

FIGURE 7. Two classical free-streamline flows: (*a*) two-dimensional Borda-mouthpiece flow; (*b*) impact of a jet on a wall. Note: in both cases the vertical line on the right (*AE* or *ED*) is the line of symmetry of the pattern. Broken lines: an arbitrary length of parallel jet may be used to join up these two flows into a limiting form of the model in figure 3 for large h/s.

The height–width ratio h/s of the half-orifice is shown by (21) and (13) to take the form

$$\frac{h}{s} = \frac{1}{\pi}\left\{\log\left[c^{\frac{1}{2}} + (c-1)^{\frac{1}{2}}\right] + \frac{(c-1)^{\frac{3}{2}}}{c^{\frac{3}{2}} + 2c - 1}\left(\tfrac{1}{2}\pi - \frac{c^{\frac{1}{2}}}{c^{\frac{1}{2}} - 1}\right)\right\}, \tag{22}$$

depending only upon c. Accordingly, equation (18) allows the induced-power coefficient C_P to be determined as the function of h/s given in figure 4.

Similarly, the form of the free streamline BC can be plotted as in figure 3 for four different values of h/s (equal to 0·6, 1·0, 1·4 and 1·8; these correspond to $c = 10{\cdot}12$, 68·2, 624 and 6855 respectively). This is done by using (12) with $0 < Z < \infty$ to trace the variation of $z = x + iy$ along the free streamline. Actually, figure 3 plots the variation of

$$[z/s]_0^Z; \tag{23}$$

accordingly, all the different free-streamline shapes in figure 3 start from the same point B (where $Z = 0$ so that (23) vanishes), and correspond to the same half-orifice width s (but to different values of the height h above ground).

For h/s taking a large value such as 3, or any greater value, the free-streamline shape is indistinguishable on the scale of figure 3 from a combination of two classical free-streamline flows (figure 7). These are the two-dimensional Borda-mouthpiece flow (see

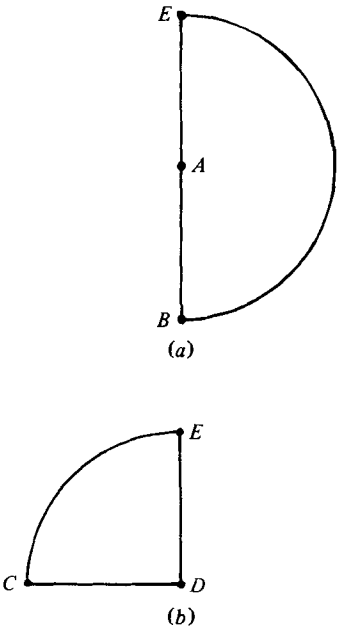

FIGURE 8. The ζ-domains corresponding to the two classical free-streamline flows of figure 7.

also the curve marked as '∞' on figure 3) forming a vertical jet at E, and the flow due to the impact of such a two-dimensional vertical jet E upon the horizontal ground at D. For these large values of h/s, the presence of the ground does not affect the induced power (so that $C_P = 1$).

Mathematically, we can see why the present solutions tend to the above limiting form by inspecting the ζ-domains (figure 8) for those two classical flows. The case $h/s \geqslant 3$ corresponds to extremely large values of $c \geqslant 10^7$. In the limit of large c, however, the corresponding ζ-domain in figure 6(b) becomes more and more a combination of those in figure 8 as E moves up closer to the circular boundary. Furthermore, the mapping of that ζ-domain onto the Z-domain degenerates in two different parts of the Z-domain into the different mappings appropriate to figures 8(a) and 8(b).

In fact, where Z remains of order 1 as $c \to \infty$, equation (10) becomes

$$\frac{dw}{dz} = \zeta = iU\frac{Z^{\frac{1}{2}} - i}{Z^{\frac{1}{2}} + i}, \tag{24}$$

which maps the upper half Z-plane onto the semicircle of figure 8(a) with $Z = -1$ and $Z = 0$ corresponding to A and B (and $Z = \infty$ to E). Equation (24) represents the Borda-mouthpiece flow without ground effect; the corresponding form of z is calculated from (11) as

$$z = \frac{Q}{\pi U}\left\{-i\log(Z^{\frac{1}{2}} - i) - \frac{1}{Z^{\frac{1}{2}} - i}\right\} + \text{constant}, \tag{25}$$

and this is seen to be equivalent to a limiting form of (12) as $c \to \infty$ for fixed Z.

By contrast, when Z/c remains fixed as $c \to \infty$, equation (10) becomes

$$\zeta = -U\left(\frac{Z^{\frac{1}{2}} - ic^{\frac{1}{2}}}{Z^{\frac{1}{2}} + ic^{\frac{1}{2}}}\right)^{\frac{1}{2}}, \tag{26}$$

which maps the upper half Z-plane onto the quadrant of figure 8(*b*) with $Z = -c$ and $Z = 0$ corresponding to D and E (and $Z = \infty$ to C). Equation (26) represents the impact of a jet on the ground; the corresponding form of z is found from (11) (where, however, $Z+1$ is to be replaced by Z since Z is of order c) as

$$z = \frac{Q}{\pi U}\left\{i \log\left[\frac{(Z+c)^{\frac{1}{2}}+c^{\frac{1}{2}}+Z^{\frac{1}{2}}}{(Z+c)^{\frac{1}{2}}-c^{\frac{1}{2}}+Z^{\frac{1}{2}}}\right] - \log\left[(Z+c)^{\frac{1}{2}}+Z^{\frac{1}{2}}\right]\right\} + \text{constant}, \tag{27}$$

and this is seen to be equivalent to a limiting form of (12) as $c \to \infty$ for fixed Z/c.

On the other hand, for more moderate values of c, there is no separation of the jet into a contracting portion (figure 7*a*) and an expanding portion (figure 7*b*). The two portions merge, so that the contraction is by no means completed by the time that the expansion begins. This leads to the 'apparent paradox' mentioned at the end of § 2: the minimum jet cross-section is *not so much reduced* as in the case without ground, even though in the latter case the flux Q is greater.

We now conclude by probing this apparent paradox a little further. We start from a balance of the supported weight W against the combined pressure force and momentum flux acting at the jet's narrowest cross-section, which we continue to denote by A as in the classical case of figure 1. This gives, to a close approximation,

$$W \doteqdot \int_A (p_e + \rho q^2)\, dA \tag{28}$$

both in the axisymmetric and two-dimensional cases (provided that, in the latter case, quantities like W and A are taken as values per unit breadth). The only approximation involved in (28) is that the fluid's speed q has been written instead of the downward component of fluid velocity, but the error is likely to be small at the jet's minimum cross-section. By (14), equation (28) can be re-written as

$$W \doteqdot \int_A \tfrac{1}{2}(\rho U^2 + \rho q^2)\, dA. \tag{29}$$

Now, as h/s progressively decreases, the streamline curvatures at cross-section A become greater, leading to enhanced excess pressure p_e and reduced fluid speeds q in the centre of the jet. Equation (29) means therefore that the area A necessary to support the weight W progressively *increases*.

On the other hand, the arithmetic mean inside the integral (29) exceeds the corresponding geometric mean $\rho U q$, and by a larger margin the greater is the ratio U/q. This implies that the volume flux

$$Q \doteqdot \int_A q\, dA = \left(\int_A \rho U q\, dA\right) \Big/ \rho U \tag{30}$$

[where the approximate equality should be at least as accurate as (28)] has two properties: (i) it is *less* than $W/\rho U$ (the value which it takes in the absence of ground); (ii) it becomes less by a larger margin as h/s decreases. It follows that we should regard the progressive reduction in volume flux (and so also in induced power) as associated naturally (not 'paradoxically') with the progressive increase in minimum jet cross-section as height above ground decreases.

REFERENCES

BATCHELOR, G. K. 1967 *An Introduction to Fluid Dynamics*. Cambridge University Press.

BLAKE, R. W. 1979 The energetics of hovering in mandarin fish (*Synchropus picturatus*). To appear in *J. exp. Biol.*

BRAMWELL, A. R. S. 1976 *Helicopter Dynamics*. London: Edward Arnold.

GLAUERT, H. 1935 Airplane propellers, vol. IV, div. L of *Aerodynamic Theory* (ed. W. F. Durand). Springer.

KNIGHT, M. & HEFNER, R. A. 1941 Analysis of ground effect on the lifting rotor. *Nat. Adv. Comm. Aeron. Tech. Note* 835.

LAMB, H. 1932 *Hydrodynamics* (6th ed.). Cambridge University Press. Also New York: Dover (1945).

LIGHTHILL, J. 1975 Aerodynamic aspects of animal flight. In *Swimming and Flying in Nature* (2 vols., ed. T. Y. Wu, C. J. Brokaw and C. Brennen), pp. 423–91. New York: Plenum Press.

LIGHTHILL, J. 1977 Introduction to the scaling of aerial locomotion. In *Scale Effects in Animal Locomotion* (ed. T. J. Pedley), pp. 365–404. London: Academic Press.

RAYNER, J. M. V. 1979 A vortex theory of animals flight. Part 1. The vortex wake of a hovering animal. *J. Fluid Mech.* **91**, 397–730.

THEODORSEN, T. 1969 Theory of static propellers and helicopter rotors. *Proc. 25th Ann Nat. Forum Amer. Helicopter Soc.* p. 236.

WEIS-FOGH, T. 1973 Quick estimates of flight fitness in hovering animals, including novel mechanisms for lift production. *J. Exp. Biol.* **59**, 169–230.

ZBROZEK, J. 1950 Ground effect on the lifting rotor. *Aero. Res. Counc. Rep. and Memor.* no. 2347. London: Her Majesty's Stationery Office.

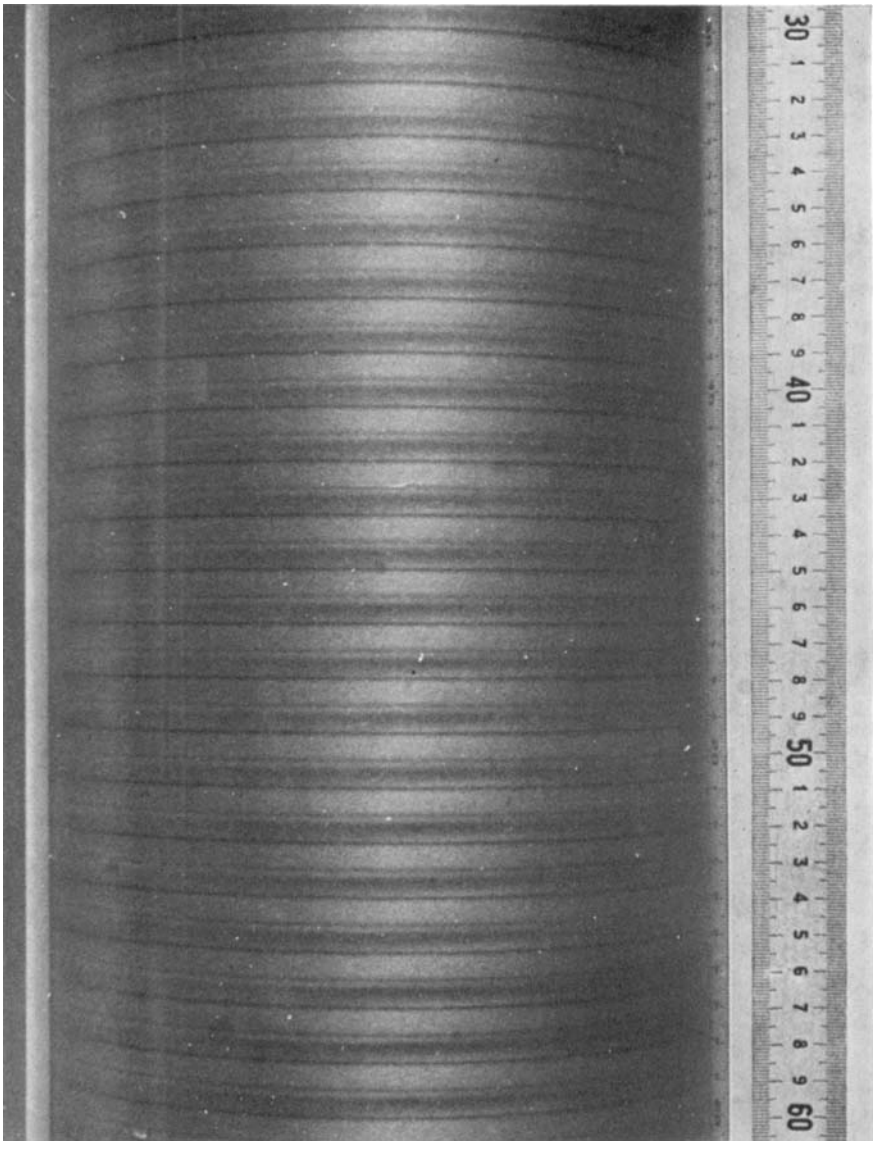

FIGURE 1. Centre section of the fluid column with laminar axisymmetric Taylor vortices in silicone oil at $T = 1{\cdot}16T_c$ with $\lambda = 2{\cdot}13$. Narrow gap. The heavy dark lines are the sinks, the location of inward fluid motion. The fine dark lines are the sources, the location of outward fluid motion.

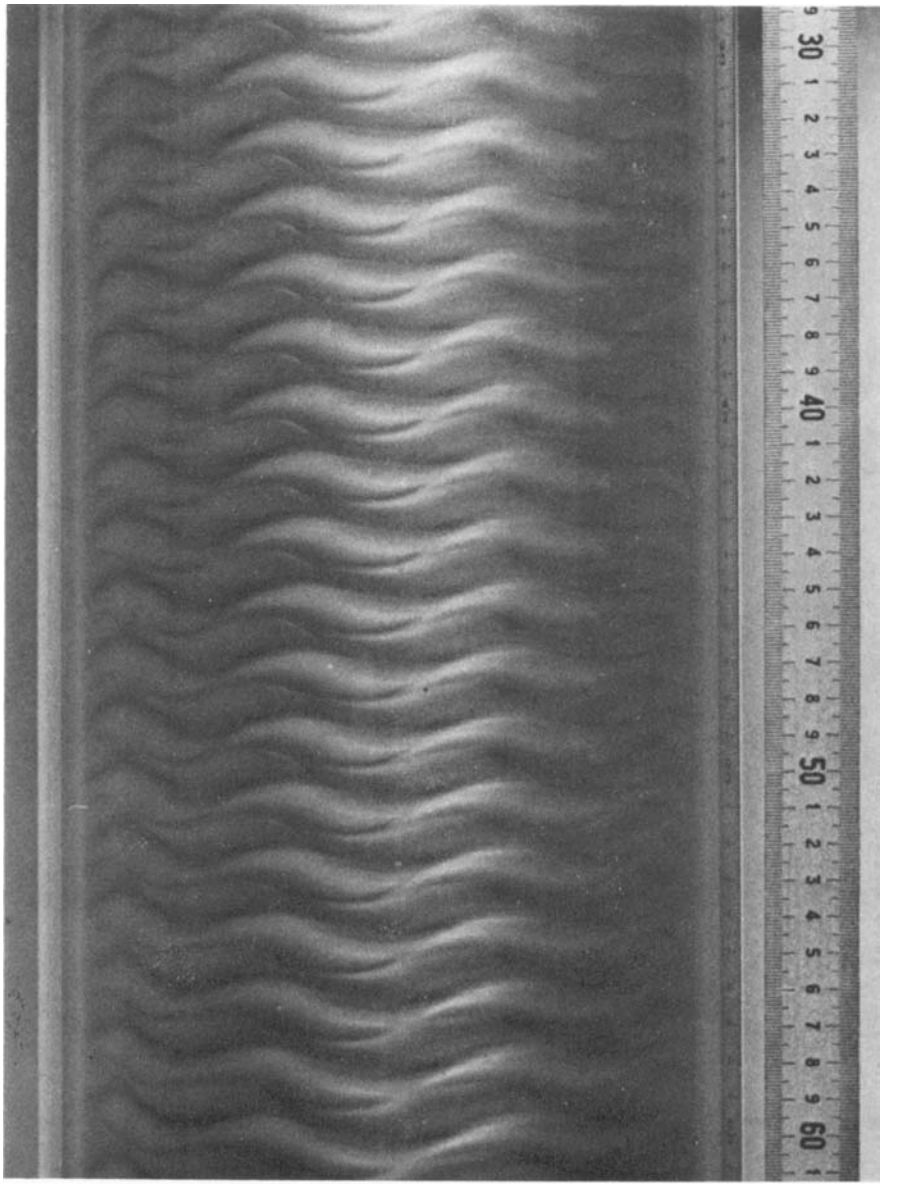

FIGURE 2. Centre section of the fluid column with laminar doubly periodic Taylor vortices in water in the narrow gap. $T = 8{\cdot}49T_c$, $\lambda = 2{\cdot}60$, six azimuthal waves.

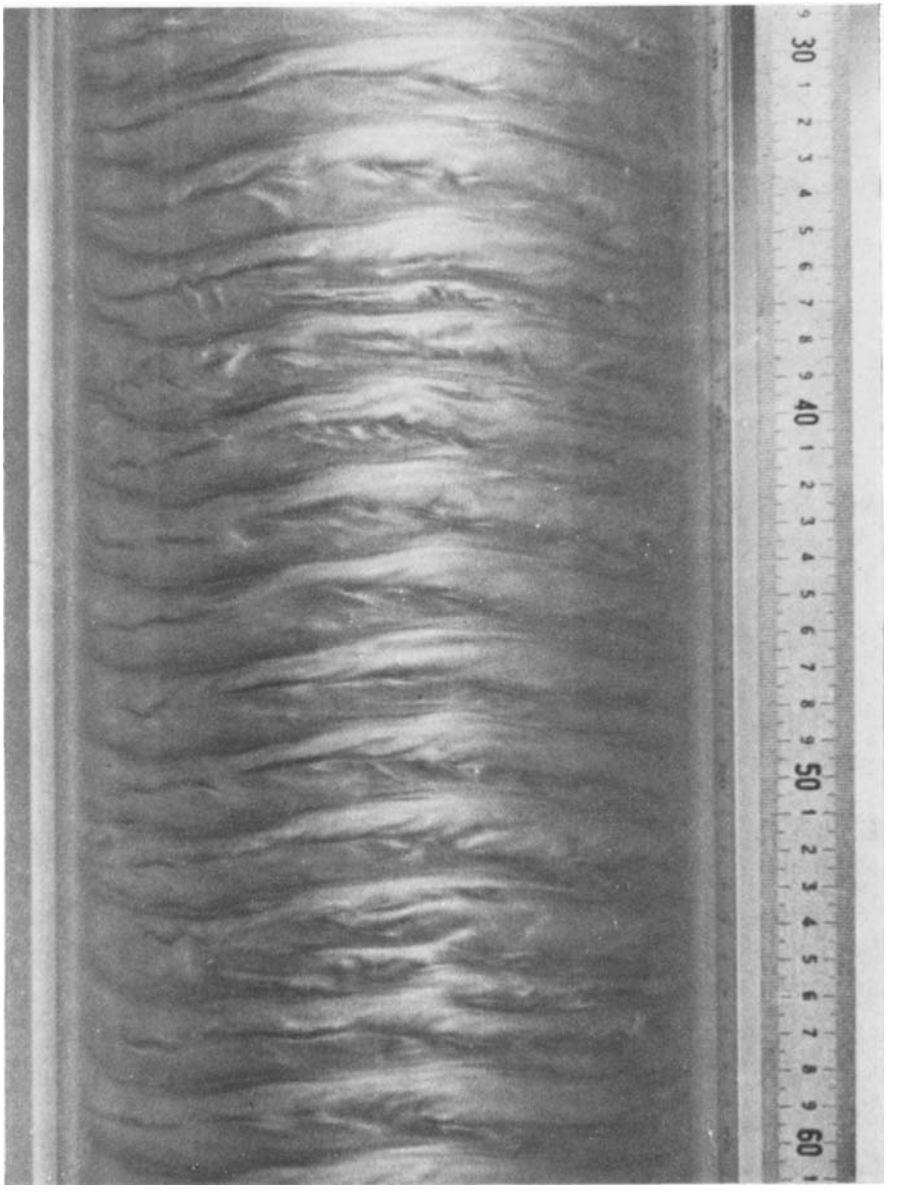

FIGURE 4. Centre section of fluid column at $T = 120T_c$ with maximal wavelength $\lambda = 3{\cdot}395$ and two azimuthal waves, after a steady acceleration experiment. Transition to turbulence with transient disturbances of the flow.

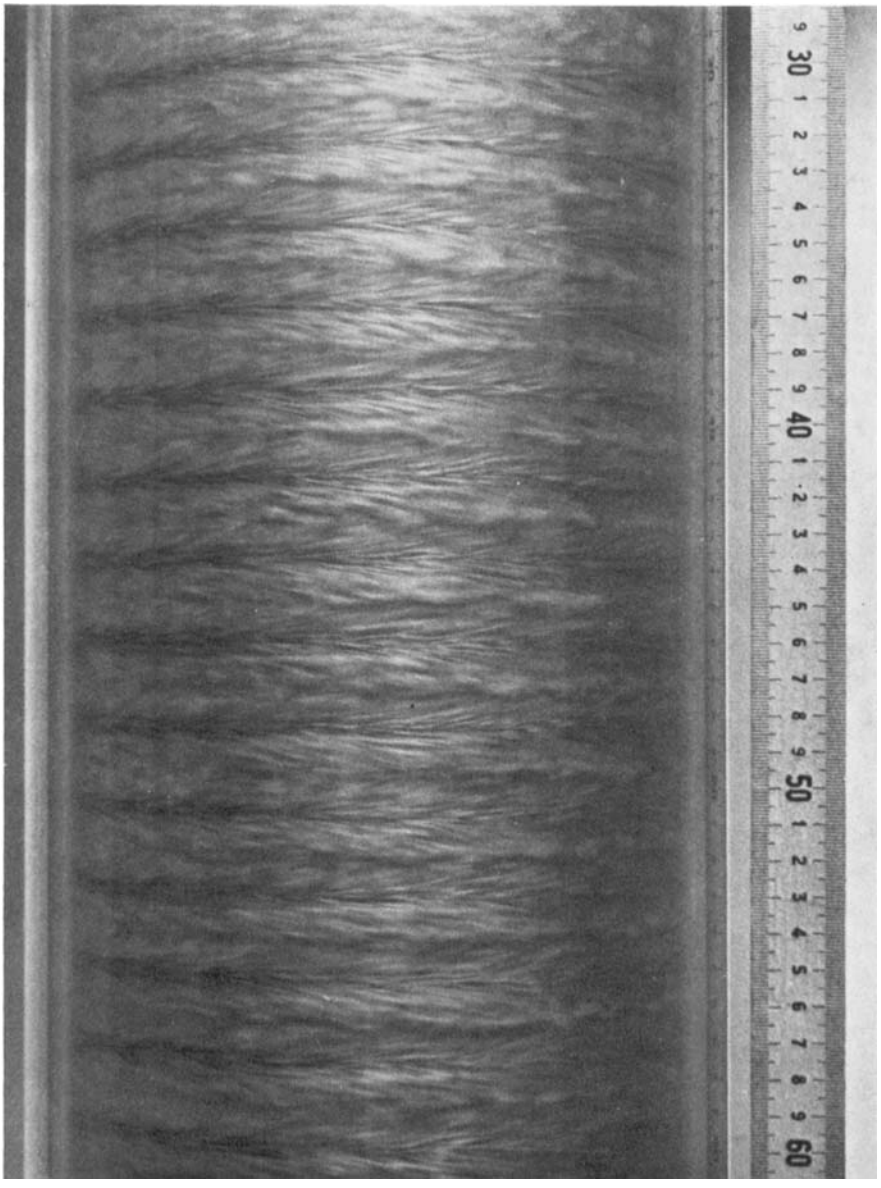

FIGURE 5. Centre section of column of turbulent axisymmetric Taylor vortices in water at $T = 3800T_c$, $\lambda = 3{\cdot}395$. In narrow gap after a steady acceleration experiment. The equally spaced horizontal lines at which the flow convergos are the sinks. The sources are diffuse. Each ring represents a vortex pair.

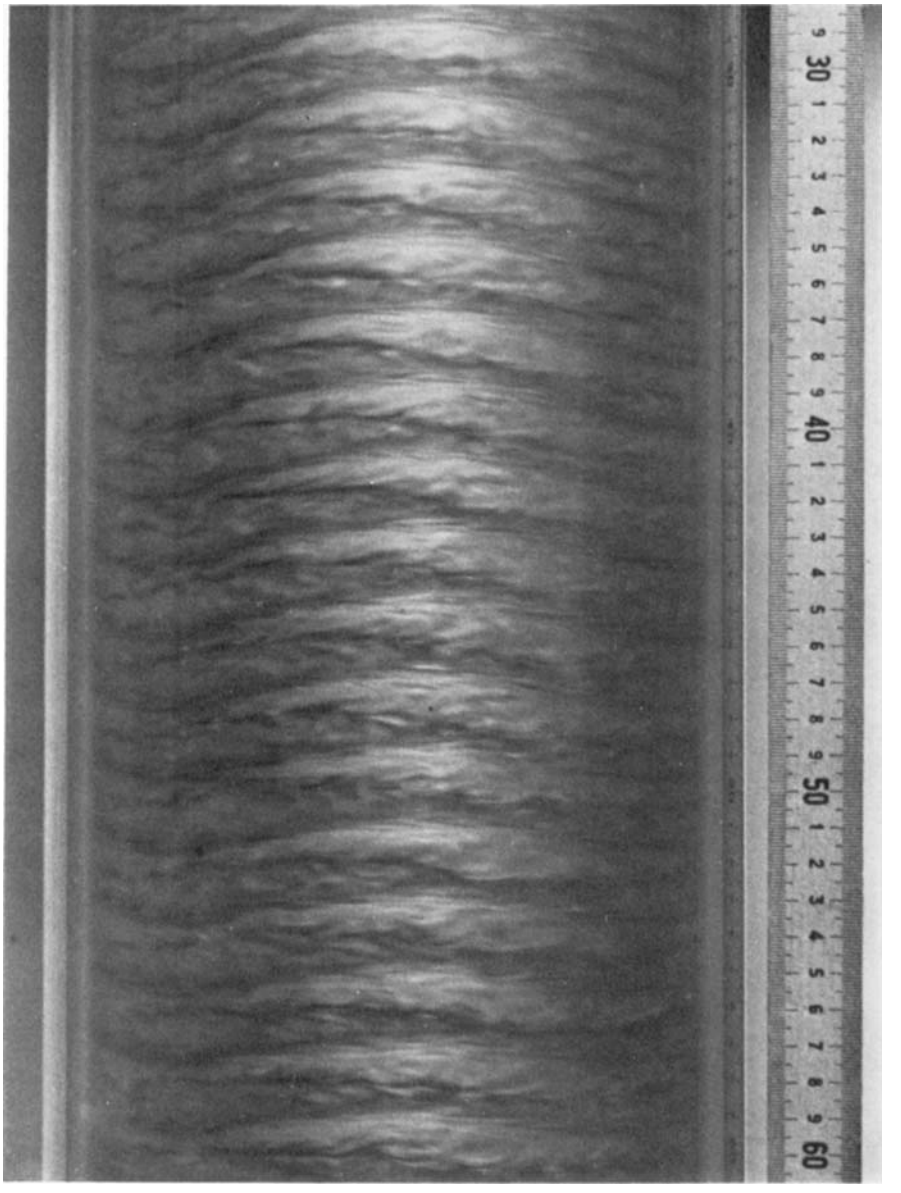

FIGURE 6. Centre section of column of steady doubly periodic turbulent Taylor vortices after a sudden start, two azimuthal waves. $T = 293T_c$, $\lambda = 2{\cdot}84$, in water with narrow gap.

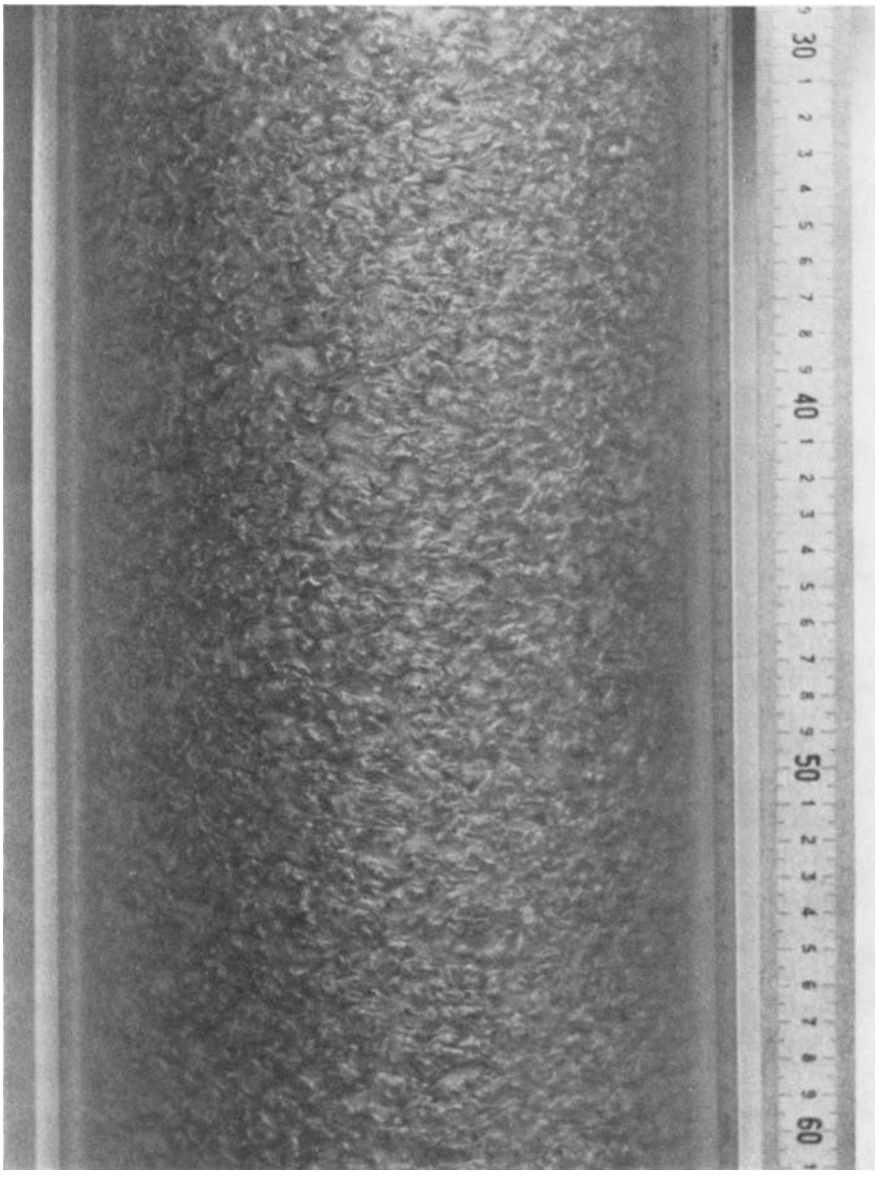

FIGURE 7. Chaotic turbulent flow arriving at the outer glass cylinder 0·5 s after sudden start at $T = 1660T_c$. In water with the narrow gap.

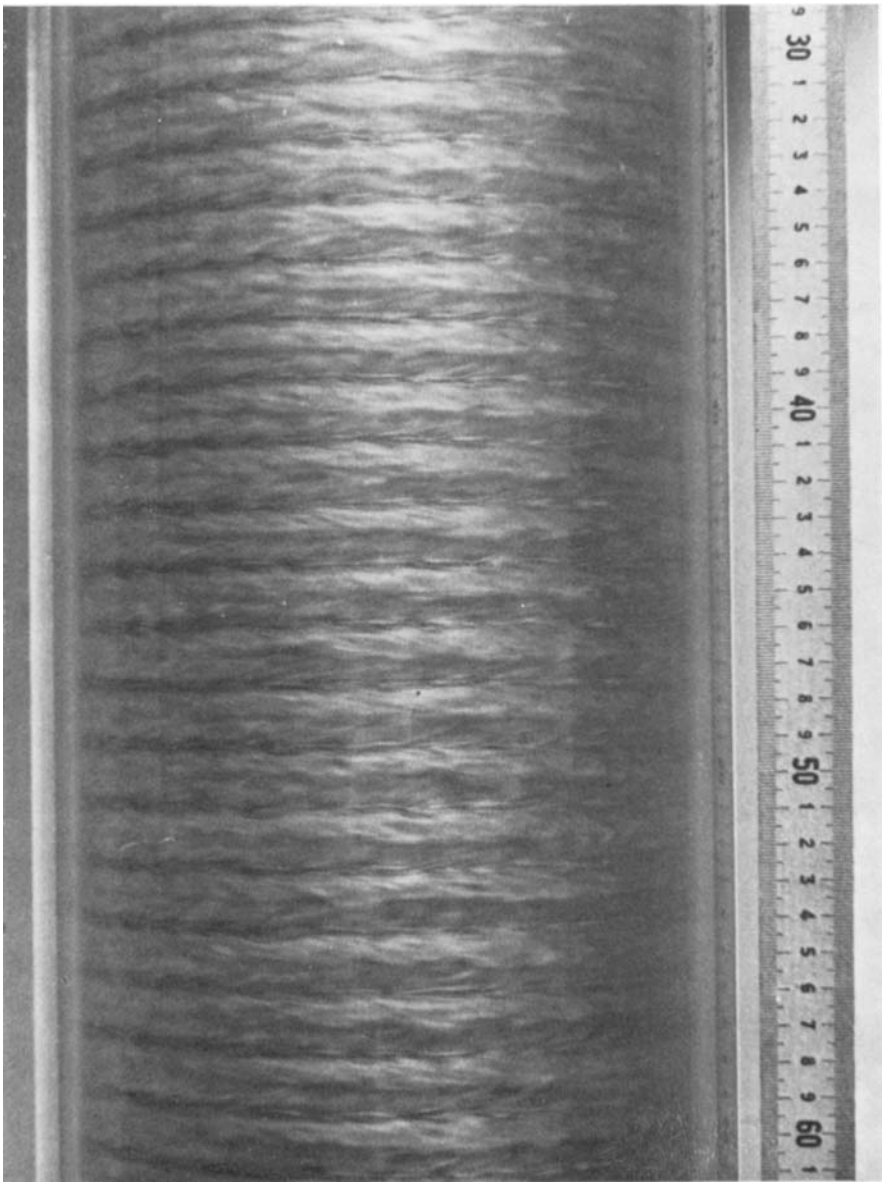

FIGURE 8. Centre section of column of turbulent axisymmetric Taylor vortices in steady state after a sudden start at $T = 1625T_c$. $\lambda = 2{\cdot}396$, narrow gap.

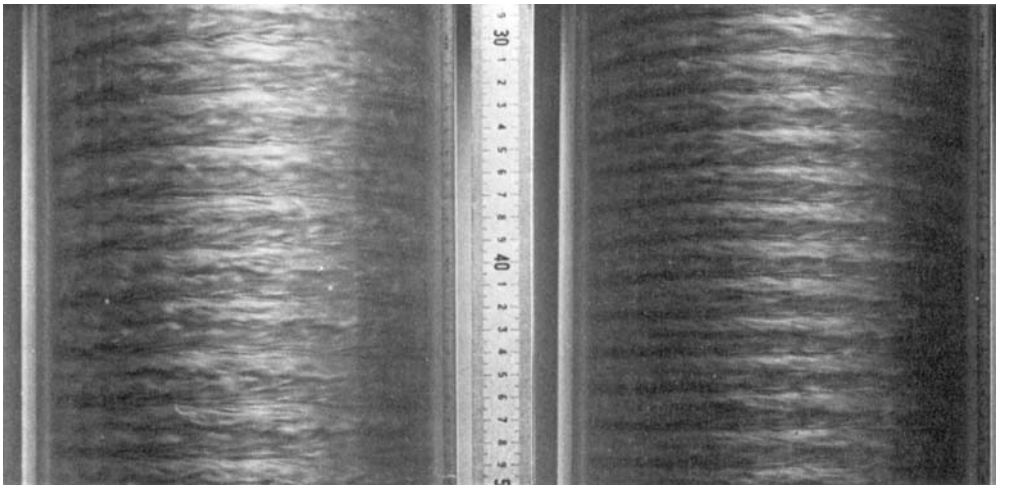

FIGURE 10. Demonstration of the non-uniqueness of turbulent axisymmetric Taylor vortex flow in the narrow gap at $T = 1650T_c$. Left steady acceleration experiment with $\lambda = 3{\cdot}395$, right steady state after sudden start at the same Taylor number with the same fluid (water), $\lambda = 2{\cdot}396$.